AIAA-91-1552-CP

Characteristic Time-Stepping or Local Preconditioning of the Euler Equations

Bram van Leer*
Wen-Tzong Lee†
and Philip Roe‡

Department of Aerospace Engineering
The University of Michigan
Ann Arbor, MI 48109-2140

Abstract

A local preconditioning matrix for the multi-dimensional Euler equations is derived that reduces the spread of the characteristic speeds from a factor $(M+1)/\min(M, |M-1|)$ to a factor $1/\sqrt{1-\min(M^2, M^{-2})}$, where M is the Mach number. It is shown that the latter value is the lowest attainable. Numerical experiments with this preconditioning, applied to an explicit upwind discretization of the two-dimensional Euler equations, show that it significantly increases the rate of convergence to a steady solution, as predicted theoretically. Other benefits expected from the use of the new preconditioning are discussed.

1 Introduction

When marching in time with an explicit Euler code, there are three distinct choices for the time-step.

1. **Global time-step**: in all computational cells the same value of Δt is used. This yields time-accuracy of the numerical solution.

2. **Local time-step**: each cell gets its own Δt_{ijk}, scaling with the maximum time-step that ensures local stability. This yields a uniform Courant number for all cells. Time-accuracy is lost, but marching to a steady state is accelerated, and the Euler schemes can be designed such that the *steady* solution is not affected.

   Using a local time-step is equivalent to preconditioning the residual by a *scalar*; the preconditioning removes the stiffness due to spatial variations in the largest characteristic speed and in cell size.

*Professor, Member AIAA
†Graduate Research Assistant, Member AIAA
‡Professor, Member AIAA

3. **Characteristic time-step**: each characteristic variable is updated with its own $\Delta t^{(l)}_{ijk}$. This is equivalent to preconditioning by a local *matrix*; it takes away the stiffness due to the variation among the local characteristic speeds, while the effect of cell aspect-ratio can also be neutralized. Time-accuracy is even further lost, but convergence to the steady state, especially to subsonic and transonic solutions, may be accelerated dramatically.

   Characteristic time-stepping may be used in tandem with local time-stepping for the maximum effect.

For the one-dimensional Euler equations, the construction of an effective matrix preconditioner is relatively simple, because the characteristic speeds and directions are known without ambiguity. For the multi-dimensional equations the situation is much complicated by the omni-directional propagation of acoustic information: there is no unique decomposition of the flow field in terms of discrete waves.

In this paper a new result for the 2-D and 3-D Euler equations is presented, in the form of a local preconditioning matrix that reduces the condition number of the characteristic speeds from $(M+1)/\min(M,|M-1|)$ to $1/\sqrt{1-\min(M^2,M^{-2})}$, where M is the Mach number; this can be shown to be the *lowest* condition number attainable. Numerical results for 2-D subsonic, transonic and supersonic flow over an airfoil are presented that fully confirm the expectation of accelerated convergence to the steady solution.

Other potential benefits of the use of the preconditioning matrix relate to its ability to make the system of the Euler equations - and discrete approximations thereof - behave more as a *scalar* equation; these are also briefly discussed.

2 Preconditioning the one-dimensional Euler equations

2.1 Analysis

The quasi-one-dimensional Euler equations for flow in a channel of variable cross-section can be written as

$$\frac{\partial \mathbf{U}}{\partial t} = -\mathbf{A}(\mathbf{U})\frac{\partial \mathbf{U}}{\partial x} + \mathbf{s}(\mathbf{U},x) = \mathbf{Res}(\mathbf{U}); \quad (1)$$

for the present analysis the conservation form is not required. Using a local time-step for these equations is equivalent to using a global time-step for the Euler equations preconditioned by a scalar:

$$\frac{\partial \mathbf{U}}{\partial t} = [\max_x r(\mathbf{A})]\,[r(\mathbf{A})]^{-1}\,\mathbf{Res}; \quad (2)$$

here $r(\mathbf{A})$ is the spectral radius of $\mathbf{A}$. Furthermore, using characteristic time-steps is equivalent to using a global time-step for the Euler equations preconditioned by a matrix:

$$\frac{\partial \mathbf{U}}{\partial t} = r(\mathbf{A})|\mathbf{A}|^{-1}\mathbf{Res}; \quad (3)$$

here $|\mathbf{A}|$ is the matrix with the same eigenvectors as $\mathbf{A}$ but with the absolute eigenvalues of the latter. In practice each of these eigenvalues may locally vanish, or be very small, making the inversion of $|\mathbf{A}|$ impossible or undesirable. Therefore, Equation (1) will actually be preconditioned according to

$$\frac{\partial \mathbf{U}}{\partial t} = r(\mathbf{A})\,(|\mathbf{A}|^*)^{-1}\,\mathbf{Res}, \quad (4)$$

where the eigenvalues of $|\mathbf{A}|^*$ are bounded away from zero. The lower bound of the eigenvalues of $|\mathbf{A}|^*$ must be chosen in accordance with the magnitude of the local source term, for reasons of numerical stability. The replacement of the matrix $|\mathbf{A}|$ by a non-singular matrix $|\mathbf{A}|^*$ arises also in the

numerical implementation of the so-called entropy condition for first-order hyperbolic systems. This technique is discussed in detail by the present authors in [1].

Ignoring the effect of the modification (4), the above preconditioning achieves a local condition number = 1, independent of the local value of the Mach number: all characteristic speeds are made equal in absolute value.

It is important to realize that preconditioning by $(|\mathbf{A}|^*)^{-1}$ does not change the *signs* of the characteristic speeds, and thus does not interfere with the imposition of boundary conditions at either end of the channel. In consequence, it does not alter the steady solution admitted by such boundary conditions.

When characteristic time-stepping is combined with the use of local time-steps, this equivalent to using a global time-step for the preconditioned system

$$\frac{\partial \mathbf{U}}{\partial t} = [\max_x r(\mathbf{A})]\,(|\mathbf{A}|^*)^{-1}\,\mathbf{Res}. \qquad (5)$$

2.2 Numerical convergence studies

To illustrate the power of local preconditioning, some numerical results are displayed in Figures 1 through 12. The odd-numbered figures show exact and discrete Euler solutions (Mach number) of steady flow in a converging-diverging nozzle with cosine-shaped area-function (50% constriction), for various in- and outflow conditions. The discrete solutions are obtained with a first-order upwind scheme that becomes second-order-accurate in the steady state, owing to characteristic decomposition of the source-term vector [2]. The odd-numbered figures show the corresponding convergence histories for all three different time-stepping strategies:

- constant time-step for the entire grid;
- local time-stepping (constant Courant number for the entire grid);
- characteristic time-stepping (preconditioning by local matrix) combined with local time-stepping.

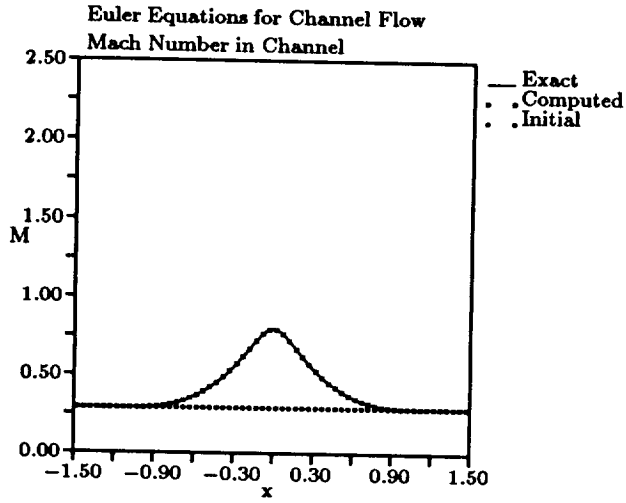

Figure 1: Subsonic solution of the Euler equations for flow in a converging-diverging channel; shown are Mach-number distributions

The savings in number of iterations with characteristic time-stepping, compared to local time-stepping, run from a factor 3 (transonic shocked flow) to 10 (supersonic, almost sonic flow). The actual savings in computing time are somewhat less, as the preconditioning technique requires the computation of $(|\mathbf{A}|^*)^{-1}$ and multiplication of the residual by this matrix.

Figures 13 and 14 illustrate an application of the preconditioning technique to a problem of *viscous* flow, namely, the self-similar hypersonic (Mach 7.95) flow over a cone also used as a test case in [3] and [4]. The terms describing the effects of viscosity and heat conduction are regarded as source terms, and determine the threshold level of the eigenvalues of the matrix $|\mathbf{A}|^*$. The discrete distribution of normalized temperature with angle coor-

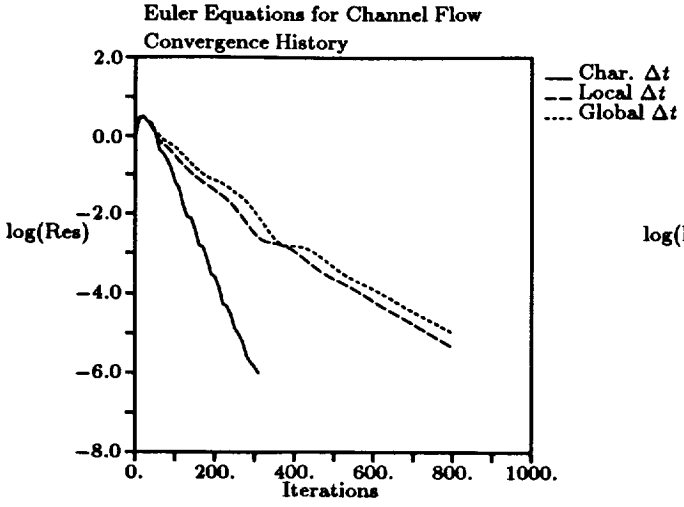

Figure 2: Convergence histories for the computation of Figure 1, for three different time-stepping techniques

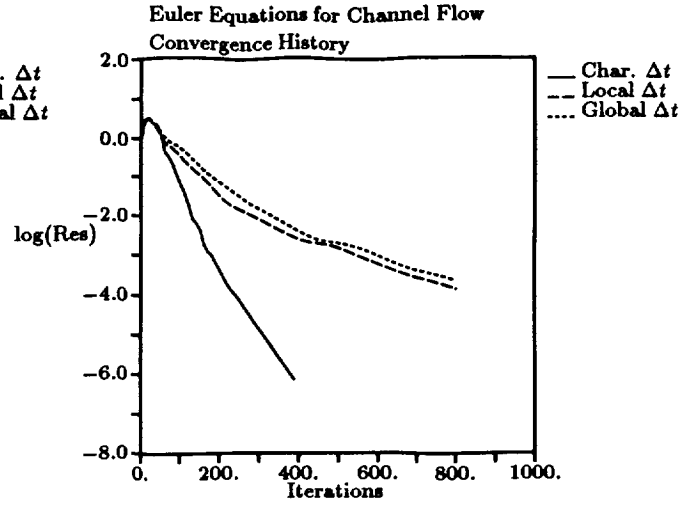

Figure 4: Convergence histories for the computation of Figure 3, for three different time-stepping techniques

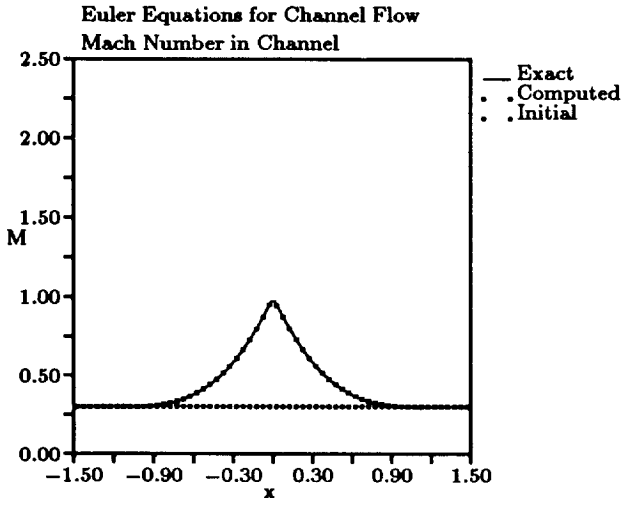

Figure 3: Subsonic, nearly sonic solution of the Euler equations for flow in a converging-diverging channel; shown are Mach-number distributions

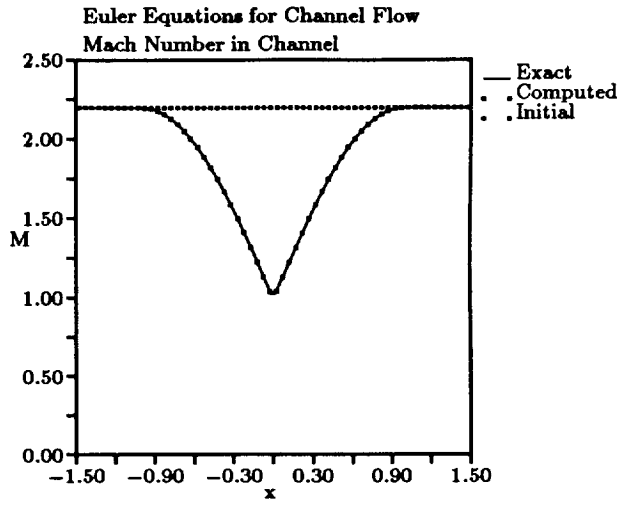

Figure 5: Supersonic, near sonic solution of the Euler equations for flow in a converging-diverging channel; shown are Mach-number distributions

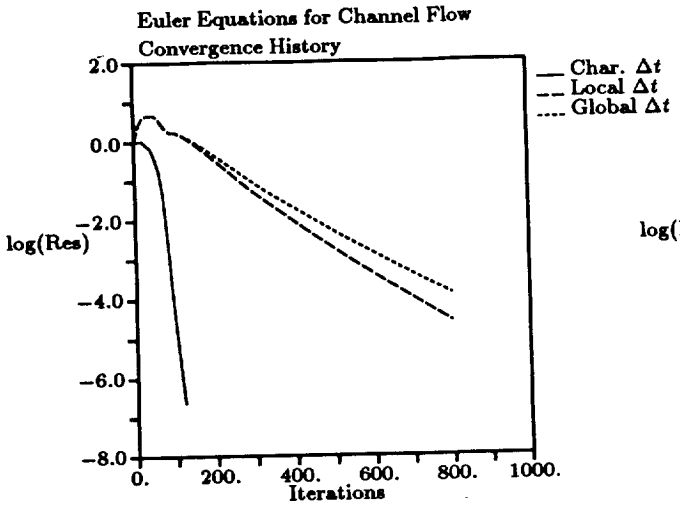

Figure 6: Convergence histories for the computation of Figure 5, for three different time-stepping techniques

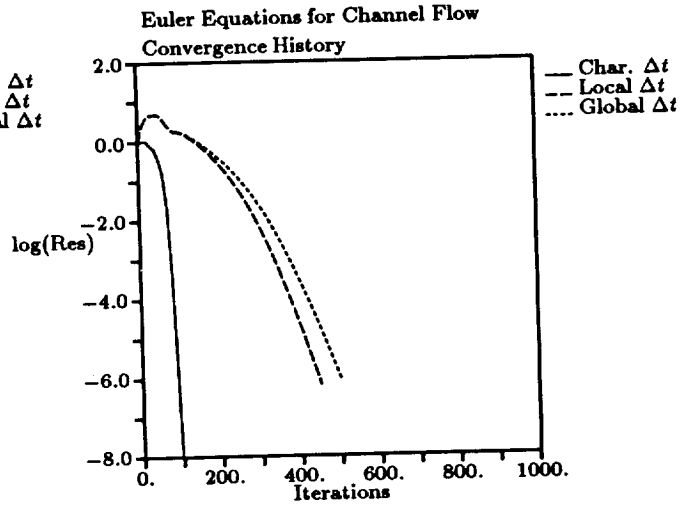

Figure 8: Convergence histories for the computation of Figure 7, for three different time-stepping techniques

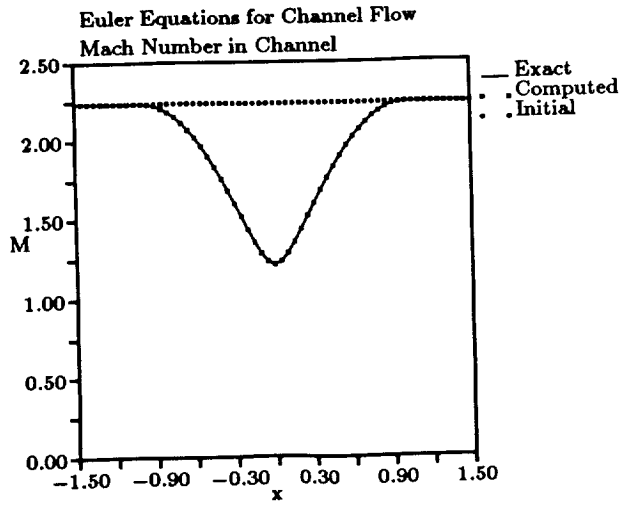

Figure 7: Supersonic solution of the Euler equations for flow in a converging-diverging channel; shown are Mach-number distributions

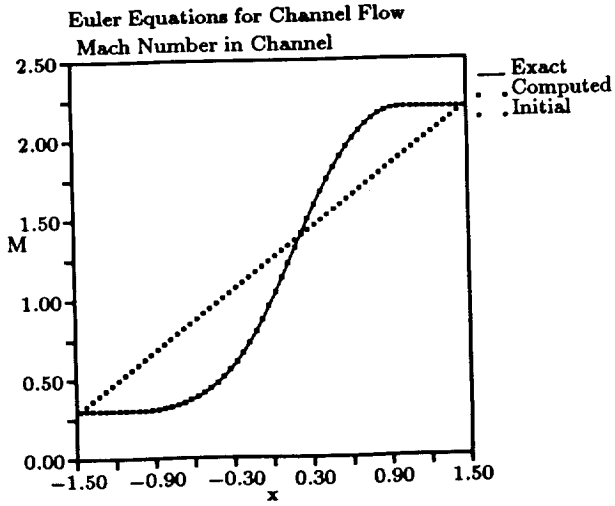

Figure 9: Transonic solution of the Euler equations for flow in a converging-diverging channel; shown are Mach-number distributions

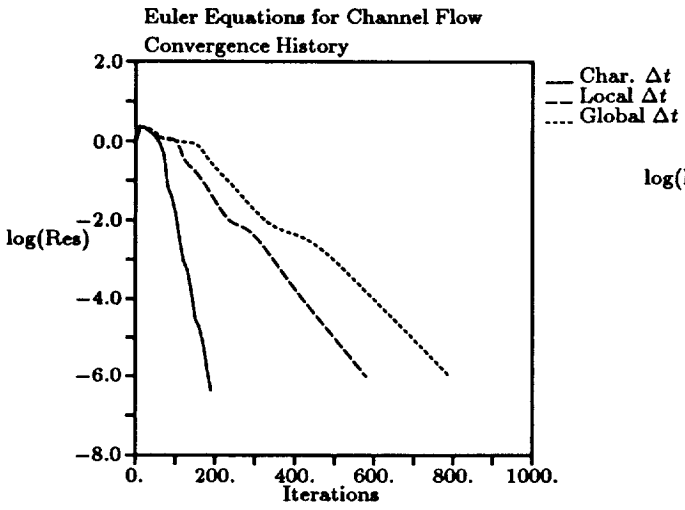

Figure 10: Convergence histories for the computation of Figure 9, for three different time-stepping techniques

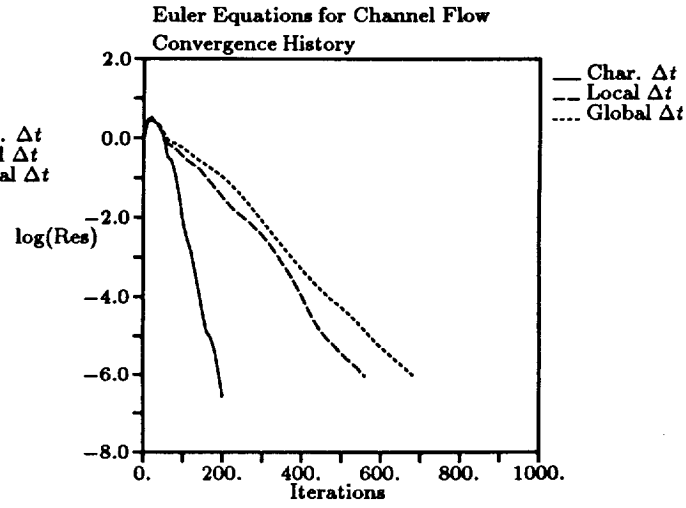

Figure 12: Convergence histories for the computation of Figure 11, for three different time-stepping techniques

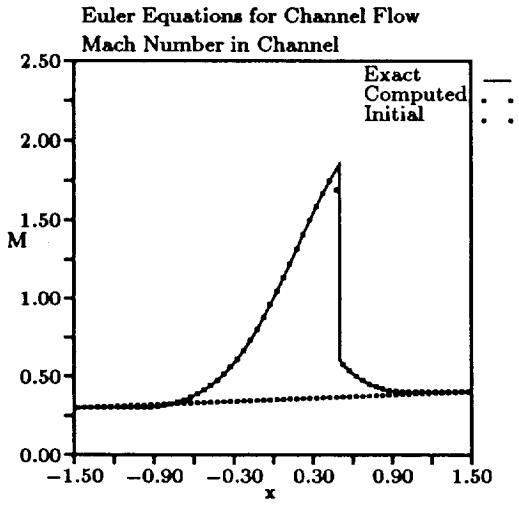

Figure 11: Transonic, discontinuous solution of the Euler equations for flow in a converging-diverging channel; shown are Mach-number distributions

dinate is shown in Figure 13; convergence histories are shown in Figure 14. The savings through preconditioning are substantial, in spite of the crudeness of the choice of preconditioning matrix. It is expected that the technique for viscous flows can still be refined.

3 Two-Dimensional Preconditioning

3.1 General features

The two-dimensional Euler equations can be written as

$$\frac{\partial \mathbf{U}}{\partial t} = -\mathbf{A}(\mathbf{U})\frac{\partial \mathbf{U}}{\partial x} - \mathbf{B}(\mathbf{U})\frac{\partial \mathbf{U}}{\partial y} = \mathbf{Res}(\mathbf{U}). \tag{6}$$

There is no obvious way to precondition the residual with a local matrix, as the matrices $\mathbf{A}(\mathbf{U})$ and $\mathbf{B}(\mathbf{U})$ do not have the same eigenvectors, and therefore can not be diagonalized simultaneously. This means Equation (6) can

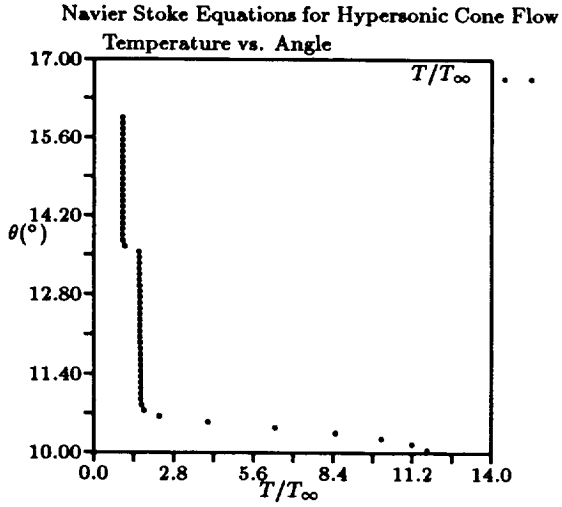

Figure 13: Numerical solution of the Navier-Stokes equations for self-similar hypersonic flow ($M_\infty = 7.95$) over a cone; shown is the non-dimensional temperature distribution.

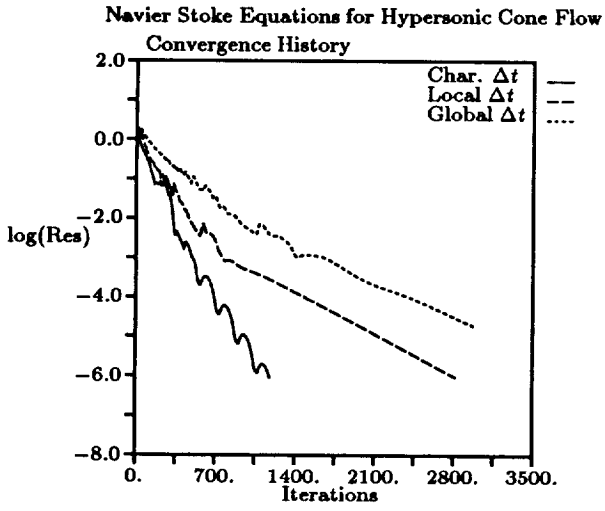

Figure 14: Convergence histories for the computation of Figure 13, for three different time-stepping techniques

not be written as a system of coupled scalar convection equations.

The derivation of a local preconditioning matrix that narrows the range of characteristic speeds for this system of equations therefore is not trivial; it is most easily understood in the case of supersonic flow. Regardless of the flow type, the analysis starts out with writing the Euler equations in a coordinate system aligned with the local flow velocity. For simplicity of notation we shall assume that this is the positive x-direction, and that the state vector $\mathbf{U}$ includes as its components pressure, two velocity components and entropy:

$$d\mathbf{U} = \begin{pmatrix} \frac{dp}{\rho a} \\ du \\ dv \\ dp - a^2 d\rho \end{pmatrix}. \qquad (7)$$

Here ρ and a denote density and sound speed, respectively. In the streamline coordinate system the matrices $\mathbf{A}$ and $\mathbf{B}$ both are symmetric:

$$\mathbf{A} = \begin{pmatrix} u & a & 0 & 0 \\ a & u & 0 & 0 \\ 0 & 0 & u & 0 \\ 0 & 0 & 0 & u \end{pmatrix}, \mathbf{B} = \begin{pmatrix} 0 & 0 & a & 0 \\ 0 & 0 & 0 & 0 \\ a & 0 & 0 & 0 \\ 0 & 0 & 0 & 0 \end{pmatrix}. \qquad (8)$$

Note that v vanishes and u equals the full flow velocity, q.

Preconditioning is now carried out in two steps:

1. **Streamwise preconditioning**, which equalizes the characteristic speeds in the streamwise direction; this is the equivalent of the 1-D preconditioning described in Section 2.1.

   Its *undesirable* effect is to exaggerate the speeds of the acoustic waves travelling normal to the flow direction; this makes the second step necessary.

2. **Normal preconditioning**, which slows down the acoustic waves travelling normal to the flow.

3.2 Supersonic case

For supersonic flow the first preconditioning is accomplished by the matrix $\mathbf{A}^{-1}$ (= $|\mathbf{A}|^{-1}$), just as in the 1-D case. The once-preconditioned equations read

$$\frac{\partial \mathbf{U}}{\partial t} = -\mathbf{A}^{-1}\left(\mathbf{A}\frac{\partial \mathbf{U}}{\partial x} + \mathbf{B}\frac{\partial \mathbf{U}}{\partial y}\right) \quad (9)$$

$$= -\left(\mathbf{I}\frac{\partial \mathbf{U}}{\partial x} + \mathbf{A}^{-1}\mathbf{B}\frac{\partial \mathbf{U}}{\partial y}\right). \quad (10)$$

This system - unlike the original Euler equations (6) - does allow representation by four pure convection equations; these can be obtained by a change of state quantities. The x-components of the convection velocities all equal unity, while the y-components are the eigenvalues of $\mathbf{A}^{-1}\mathbf{B}$, which for supersonic flow are known to be real. The effect of the first preconditioning on the wave-propagation properties of the Euler equations is illustrated in Figures 15 and 16. Note, in particular, that the acoustic wave front collapses onto two point disturbances moving at angles μ and $-\mu$, where

$$\mu = \arctan\frac{1}{\sqrt{M^2-1}} \quad (11)$$

is the Mach angle. We shall introduce the notation

$$\beta = \sqrt{M^2-1}. \quad (12)$$

The full propagation speed of the acoustic disturbances equals M/β, which increases beyond any limit as M approaches unity. The second preconditioning takes care of this problem: it reduces the acoustic wave speeds by a factor τ,

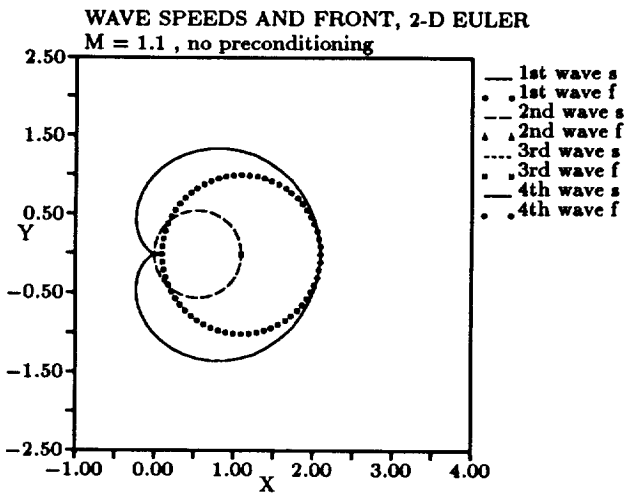

Figure 15: Polar plot of plane-wave speeds (lines) and their envelopes (symbols) for $M = 1.1$, for the original Euler equations. The speeds of *plane* waves (s in legend) moving at an angle θ are the eigenvalues of $\mathbf{A}\cos\theta + \mathbf{B}\sin\theta$; the envelopes represent the wave fronts (f in legend) produced by a *point* disturbance. Waves #1 and #4 are sound waves, #2 is an entropy wave, and #4 is a shear wave.

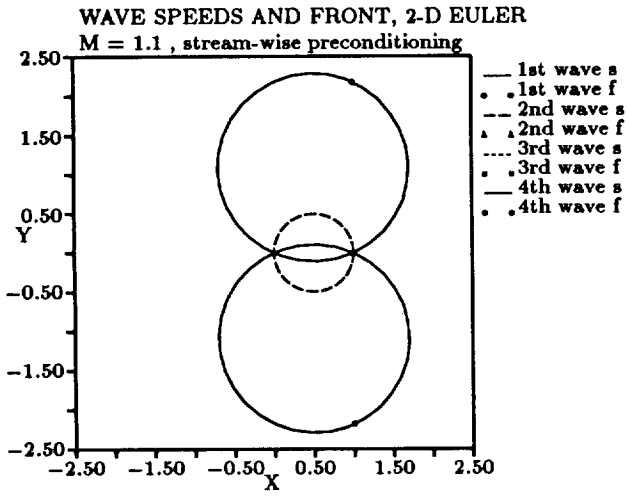

Figure 16: Polar plot of plane-wave speeds (lines) and their envelopes (symbols) for $M = 1.1$, for the Euler equations after streamwise preconditioning. For further details see the caption to Figure 15.

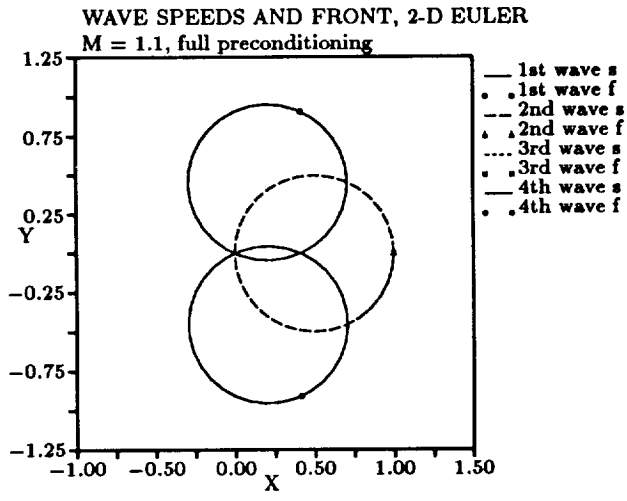

Figure 17: Polar plot of plane-wave speeds (lines) and their envelopes (symbols) for $M = 1.1$, for the Euler equations after full preconditioning. For further details see the caption to Figure 15.

$$\tau = \frac{\beta}{M} = \sqrt{1 - M^{-2}}, \qquad (13)$$

without affecting the other convection speeds. The effect of the second preconditioning on the wave-propagation properties is seen in Figure 17.

The full preconditioning matrix, product of the two factors discussed above, becomes

$$\mathbf{P}_{2D} = \begin{pmatrix} \frac{\tau}{\beta^2}M^2 & -\frac{\tau}{\beta^2}M & 0 & 0 \\ -\frac{\tau}{\beta^2}M & \frac{\tau}{\beta^2}+1 & 0 & 0 \\ 0 & 0 & \tau & 0 \\ 0 & 0 & 0 & 1 \end{pmatrix}; \qquad (14)$$

note that it is symmetric. The normalization is such that all characteristic speeds equal the flow speed q.

From Figures 15 and 17 it can be seen that the region of influence of a point source of waves for the preconditioned Euler equations is contained in the region of influence for the original equations. Thus, the preconditioning does not interfere with any prescribed boundary conditions, and will not alter the steady solution admitted by such boundary conditions.

3.3 Subsonic case

The optimal preconditioning for the subsonic case is not a straightforward extension of the corresponding 1-D technique discussed in Section 2.1. Specifically, the matrix $|\mathbf{A}|^{-1}$ is *not* the right choice for the streamwise-preconditioning step. This is not so evident for M close to unity, but clearly shows when M goes to zero: the second preconditioning can not prevent the condition number for the characteristic speeds from deteriorating to $1/\sqrt{M}$.

An analysis of symmetric preconditioning matrices with the same sparsity as $\mathbf{P}_{2D}$ in Equation (14) leads to a surprising result:

The matrix $\mathbf{P}_{2D}$ is also the optimum local

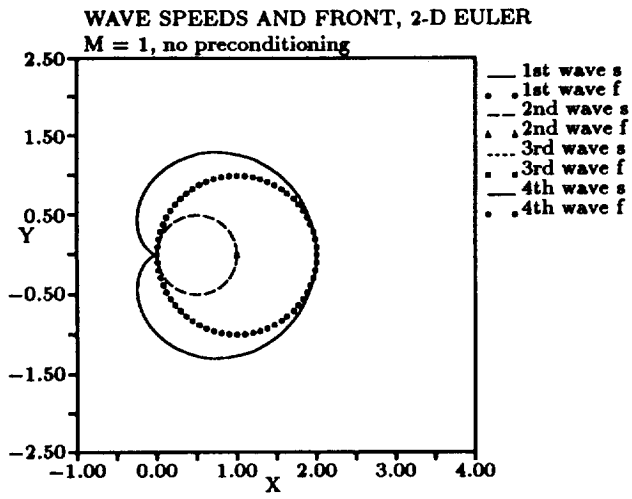

Figure 18: Polar plot of plane-wave speeds (lines) and their envelopes (symbols) for $M = 1$, for the original Euler equations. For further details see the caption to Figure 15.

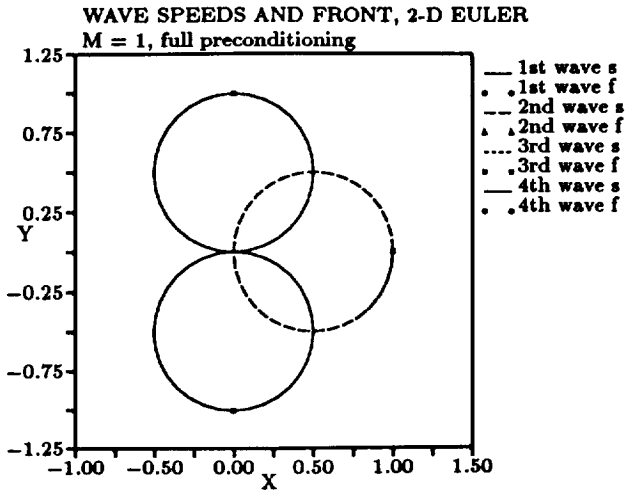

Figure 19: Polar plot of plane-wave speeds (lines) and their envelopes (symbols) for $M = 1$, for the Euler equations after full preconditioning. For further details see the caption to Figure 15.

preconditioning matrix in the subsonic case, provided that the definitions of β and τ are extended in the following way:

$$\beta = \begin{cases} \sqrt{1-M^2}, & M < 1, \\ \sqrt{M^2-1}, & M \geq 1; \end{cases} \qquad (15)$$

$$\tau = \begin{cases} \sqrt{1-M^2}, & M < 1, \\ \sqrt{1-M^{-2}}, & M \geq 1. \end{cases} \qquad (16)$$

The effect of this matrix on the wave-propagation properties of the Euler equations is illustrated by the sequence of Figures 18-27. Special attention should be given to Figure 19, which shows the wave fronts after full preconditioning in the limit of $M \downarrow 1$. The acoustic disturbances in this case are emitted at right angles to the flow direction, indicating the limit of the Mach angle. For $M < 1$ the Mach angle becomes complex, meaning that there no longer exists a pair of real propagation directions for the acoustic information. Instead, an omni-directional acoustic wave front must be invoked, even for the preconditioned equations.

How the transition occurs is seen in Figure

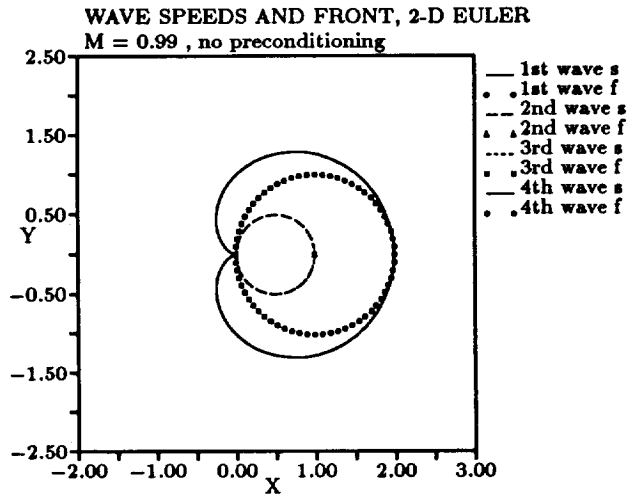

Figure 20: Polar plot of plane-wave speeds (lines) and their envelopes (symbols) for $M = 0.99$, for the original Euler equations. For further details see the caption to Figure 15.

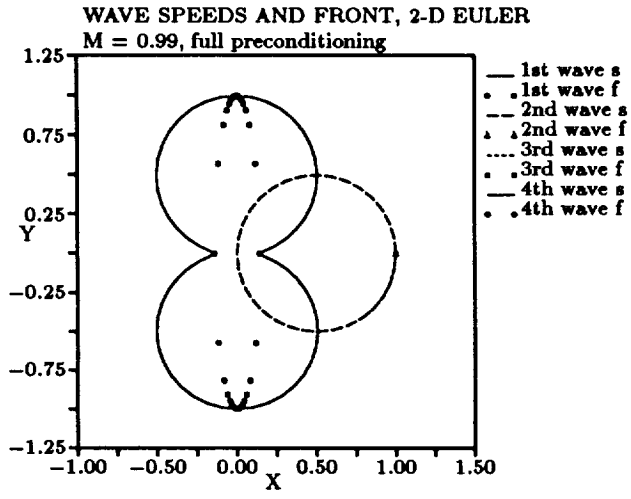

Figure 21: Polar plot of plane-wave speeds (lines) and their envelopes (symbols) for $M = 0.99$, for the Euler equations after full preconditioning. For further details see the caption to Figure 15.

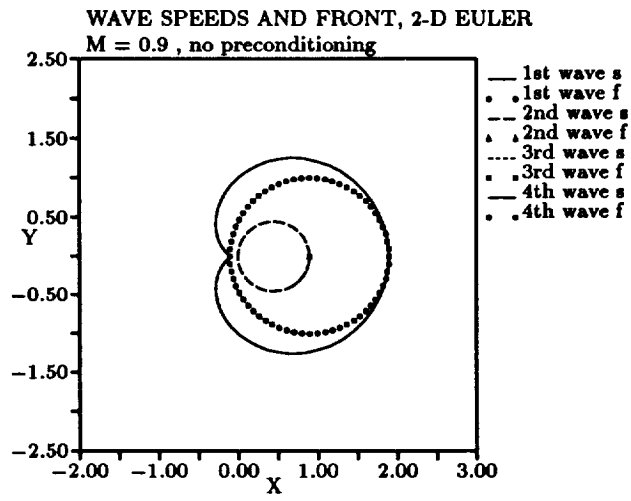

Figure 22: Polar plot of plane-wave speeds (lines) and their envelopes (symbols) for $M = 0.9$, for the original Euler equations. For further details see the caption to Figure 15.

21: the two acoustic point-disturbances from Figure 19 have become the end points of the major axis of a slender ellipse, of which the half minor axis equals τ. This means that the condition number of the characteristic speeds for $M < 1$ equals $1/\sqrt{1-M^2}$, a result that can not be improved upon, if we insist on continuity of the geometry of the acoustic wave-front when the flow changes type. Fortunately, this singularity of the condition number for $M \uparrow 1$ is an inverse-square-root singularity, which means a great improvement over the behavior of $(M+1)/(1-M)$, the condition number for the usual Euler equations.

The validity of the preconditioning matrix (14) in the limit of $M \downarrow 0$ is demonstrated by Figure 27, which shows an essentially circular acoustic wave-front travelling at the flow speed rather than the sound speed. This result improves upon the preconditioning of Turkel [5] for almost incompressible flow, which yields a condition num-

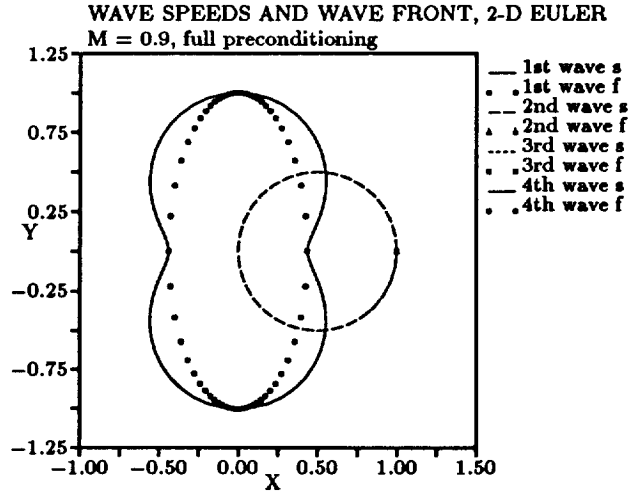

Figure 23: Polar plot of plane-wave speeds (lines) and their envelopes (symbols) for $M = 0.9$, for the Euler equations after full preconditioning. For further details see the caption to Figure 15.

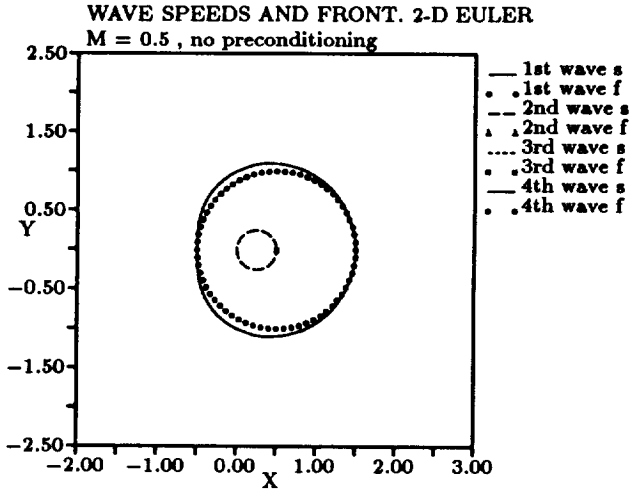

Figure 24: Polar plot of plane-wave speeds (lines) and their envelopes (symbols) for $M = 0.5$, for the original Euler equations. For further details see the caption to Figure 15.

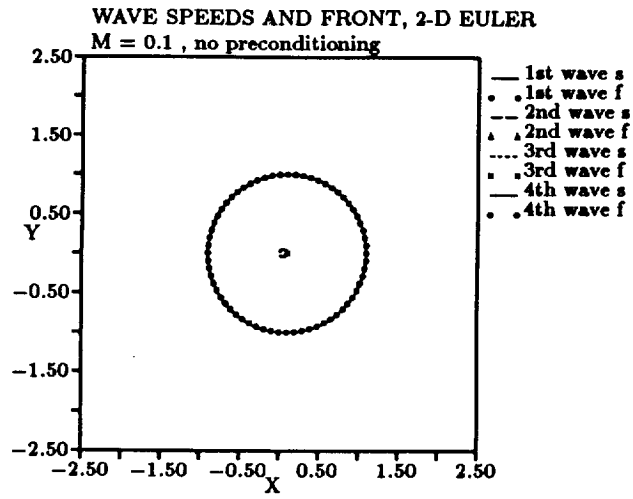

Figure 26: Polar plot of plane-wave speeds (lines) and their envelopes (symbols) for $M = 0.1$, for the original Euler equations. For further details see the caption to Figure 15.

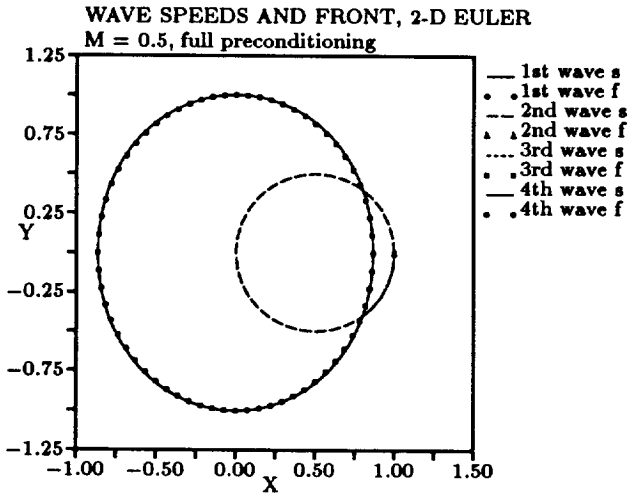

Figure 25: Polar plot of plane-wave speeds (lines) and their envelopes (symbols) for $M = 0.5$, for the Euler equations after full preconditioning. For further details see the caption to Figure 15.

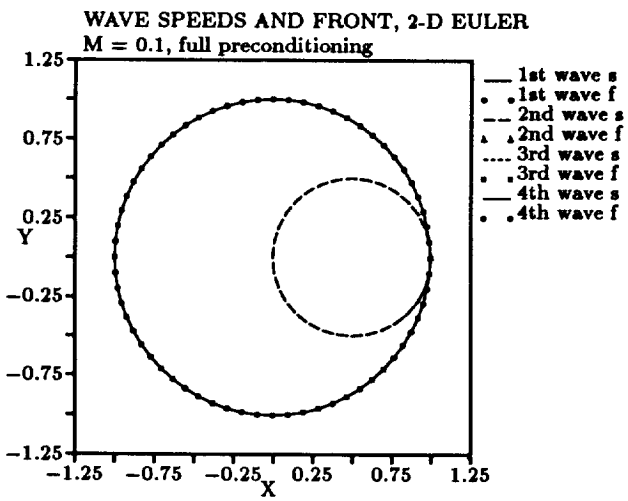

Figure 27: Polar plot of plane-wave speeds (lines) and their envelopes (symbols) for $M = 0.1$, for the Euler equations after full preconditioning. For further details see the caption to Figure 15.

ber $(\sqrt{5}+1)/(\sqrt{5}-1)$. Turkel's matrix is sub-optimal because it has non-zero elements only on the main diagonal. Later, Turkel [6] explored the use of off-diagonal elements, thereby achieving a condition number = 1 for $M \downarrow 0$. The resulting preconditioning matrix, though, lacks the general applicability of $\mathbf{P}_{2D}$.

3.4 Numerical implementation

Before it can be applied to the Euler equations under general flow conditions, the matrix $\mathbf{P}_{2D}$ must undergo two similarity transformations: one for measuring momentum in a Cartesian frame rather than a stream-aligned frame, and one for the change from the symmetrizing variables (7) to the conserved variables. Furthermore, the unboundedness of the matrix at $M = 1$ must be prevented by bounding β away from zero, as in the one-dimensional case. Because of its normalization the matrix remains bounded for $M \downarrow 0$, but the local time-step value, needed to reap the benefit of the preconditioning, nominally increases as M^{-1}, and obviously must be capped at some finite value.

The next question to be addressed is: how will the preconditioning, derived for the partial differential equations, act upon the discretized equations, i.e. in the presence of a numerical truncation error? This is not an issue in one dimension, where the preconditioning matrix commutes with the flux Jacobian, but very much so in two and three dimensions, where the Jacobians commute neither with each other nor with the preconditioner.

Initial numerical experiments, in which the preconditioning was applied to a standard first-order upwind-differencing Euler scheme based on Roe's [2] flux function, indicated a severe stability restriction on the time-step. Analysis showed that this restriction could be lifted only through a modification of the numerical flux function. The bottom line is that the *preconditioned* scheme must have the form of a first-order upwind-differencing scheme for the *preconditioned* Euler equations. For Roe's flux function the modification amounts to a subtle change in the artificial-dissipation matrix.

For an illustration with formulas, assume the grid locally is stream-aligned, as in Section 3.1; the Euler equations can then be written as

$$\frac{\partial \mathbf{W}}{\partial t} = -\frac{\partial \mathbf{F}}{\partial x} - \frac{\partial \mathbf{G}}{\partial y} \tag{17}$$

$$= -\mathbf{A}_c \frac{\partial \mathbf{W}}{\partial x} - \mathbf{B}_c \frac{\partial \mathbf{W}}{\partial y}, \tag{18}$$

where $\mathbf{W}$, $\mathbf{F}$, $\mathbf{G}$, $\mathbf{A}_c$ and $\mathbf{B}_c$ represent the conserved state quantities, their fluxes, and the flux Jacobians. The upwind-biased flux in, say, the x-direction at the interface of cells L (left) and R (right) reads

$$\mathbf{F}_{\text{upwind}} = \frac{1}{2}(\mathbf{F}_L + \mathbf{F}_R) - \frac{1}{2}\left|\hat{\mathbf{A}}_c\right|(\mathbf{W}_R - \mathbf{W}_L), \tag{19}$$

where $\hat{\mathbf{A}}_c$ is the Roe-average of the Jacobian for the pair $(\mathbf{W}_L, \mathbf{W}_R)$. In case of preconditioning, the artificial-viscosity matrix $\left|\hat{\mathbf{A}}_c\right|$ must be replaced by $\hat{\mathbf{P}}_{2D}^{-1}\left|\hat{\mathbf{P}}_{2D}\hat{\mathbf{A}}_c\right|$, which is different for $M < 1$, i.e., when the eigenvalues of $\hat{\mathbf{A}}_c$ have mixed signs. The modified flux thus reads

$$\mathbf{F}_{\text{upwind}}^{\text{mod}} = \frac{1}{2}(\mathbf{F}_L+\mathbf{F}_R) - \frac{1}{2}\hat{\mathbf{P}}_{2D}^{-1}\left|\hat{\mathbf{P}}_{2D}\hat{\mathbf{A}}_c\right|(\mathbf{W}_R-\mathbf{W}_L). \tag{20}$$

After multiplication of the discrete residual by $\mathbf{P}_{2D}$ the dissipation matrix approximately becomes $\left|\hat{\mathbf{P}}_{2D}\hat{\mathbf{A}}_c\right|$ (exactly only for the linearized Euler equations), which is the proper matrix to use when formulating an upwind scheme for the preconditioned equations

$$\frac{\partial \mathbf{W}}{\partial t} = -\mathbf{P}\mathbf{A}_c \frac{\partial \mathbf{W}}{\partial x} - \mathbf{P}\mathbf{B}_c \frac{\partial \mathbf{W}}{\partial y}. \tag{21}$$

The flux in the y-direction is treated similarly, by replacing $\left|\hat{\mathbf{B}}_c\right|$ by $\hat{\mathbf{P}}_{2D}^{-1}\left|\hat{\mathbf{P}}_{2D}\hat{\mathbf{B}}_c\right|$; these matrices are different for all M, since the eigenvalues of $\hat{\mathbf{B}}_c$ always have mixed signs.

It turns out that the new matrix preconditioning does not always necessitate a modification of the numerical flux function. It was found, for instance, that no change was needed in an upwind-biased flux based on Van Leer's [7] flux-vector splitting. The same tolerance is expected of flux functions incorporating a scalar dissipation coefficient, such as used in central-differencing schemes [8].

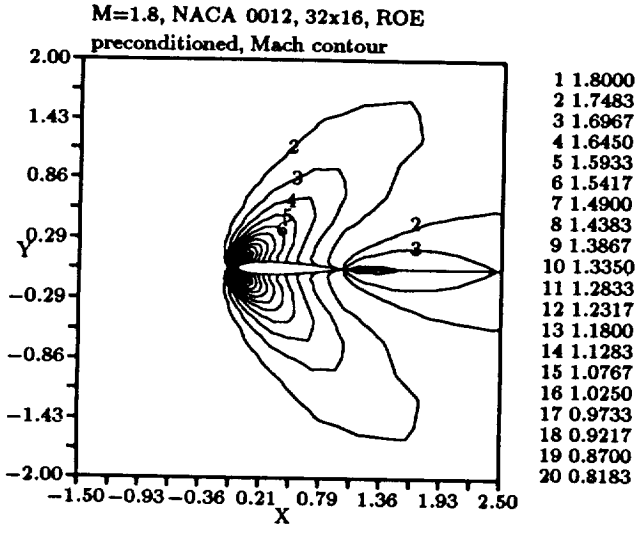

Figure 28: Steady solution of the Euler equations for flow over a NACA 0012 airfoil at $M_\infty = 1.8$, $\alpha = 0°$; shown are Mach-number contours. Matrix preconditioning was applied in combination with local time-stepping. Numerical flux function used: Roe's.

3.5 Numerical convergence studies

Numerical results illustrating the effect of local preconditioning on computing steady two-dimensional flows about a NACA 0012 airfoil are displayed in Figures 28 through 43, ordered by decreasing free-stream Mach number. The computations were made with first-order upwind differencing on a coarse O-grid (32×16 cells), so the quality of the solutions is poor; what matters, however, is how fast these solutions were obtained. In most computations Roe's flux function, or its preconditioned version, was used; only Figures 35 and 36 were based on Van Leer's flux-vector splitting. Time-marching was done by a two-stage scheme with strong high-frequency damping (see Section 6), at a local time-step corresponding to a sub-optimal Courant-number value of 0.5.

The first pair of figures of the sequence shows the solution (Mach contours) for $M_\infty = 1.8$ and $\alpha = 0°$ (zero angle of attack), obtained with the preconditioned scheme, and the residual-convergence histories for this computation (solid line) and a computation of the same flow with the regular scheme (dashed line). The steady solution in Figure 28, although crude, shows the essential features of the flow at low resolution: a smeared bow shock and an attempt to a tail shock. The free-stream characteristic condition number at Mach 1.8 is $(1.8 + 1)/(1.8 - 1) = 3.5$, although much higher values are found near the normal section of the bow shock, so a convergence acceleration by preconditioning of factor 3.5 or more might be anticipated. Such a prediction would be based on the assumption that convection of errors out of the computational domain is solely responsible for the convergence process; in reality numerical dissipation plays a role, as well as interaction of the error waves with the domain boundaries. Figure 29 shows a difference in convergence rate of a factor 3.2 after the initial transients are over, in reasonable agreement with the prediction.

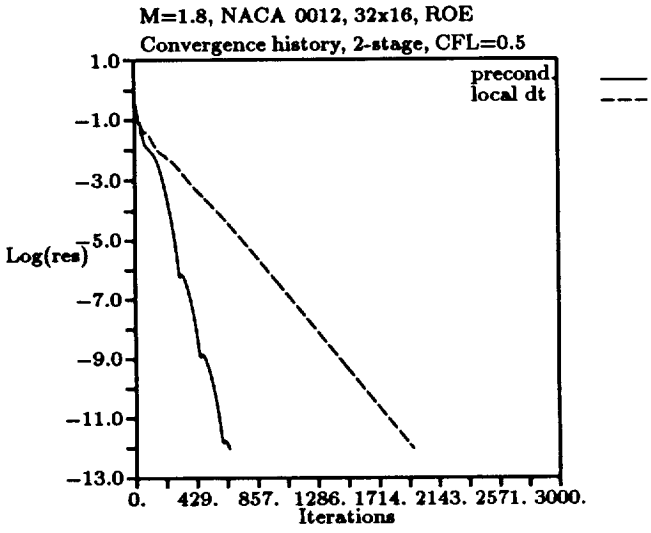

Figure 29: Residual-convergence histories for the computation of the solution of Figure 28 (solid line) and the corresponding solution without preconditioning (dashed line).

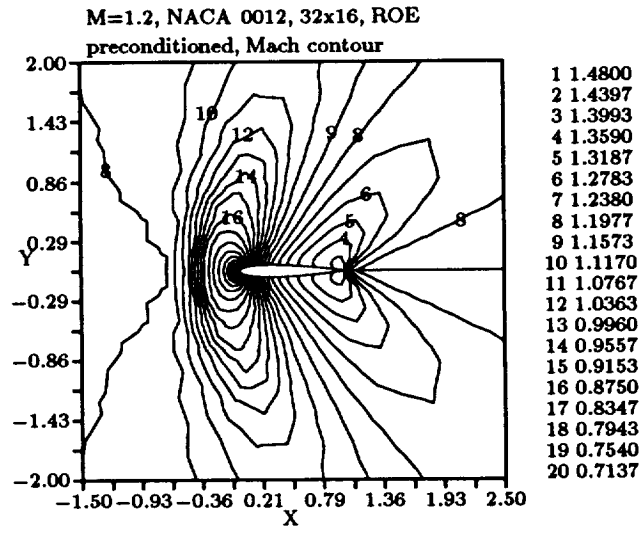

Figure 30: Steady solution of the Euler equations for flow over a NACA 0012 airfoil at $M_\infty = 1.2$, $\alpha = 0°$; shown are Mach-number contours. Matrix preconditioning was applied in combination with local time-stepping. Numerical flux function used: Roe's.

The next pair, Figures 30 and 31, shows one solution and two residual histories for $M_\infty = 1.2$, $\alpha = 0°$. Free-stream conditions would suggest a possible speed up by preconditioning of a factor 12; in reality the speed-up is about a factor 6.

Figures 32 to 36 all concern the transonic lifting flow defined by $M_\infty = 0.85$, $\alpha = 1.0°$, a well-known AGARD test-case [9]. The first trio shows both solutions, regular and after preconditioning, with Roe's flux, and the corresponding residual histories. The two solutions are somewhat different, because of the different dissipation matrices used in the two discretizations. Both capture the transonic regions terminated by normal shocks; the solution by the preconditioned scheme shows signs of a large entropy error at the airfoil surface (bending of Mach contours). The free-stream condition numbers are 12.3 before and $1/\sqrt{(1-0.85^2)}$=1.90 after preconditioning, suggesting a possible convergence acceleration of a factor 6.5; the actual con-

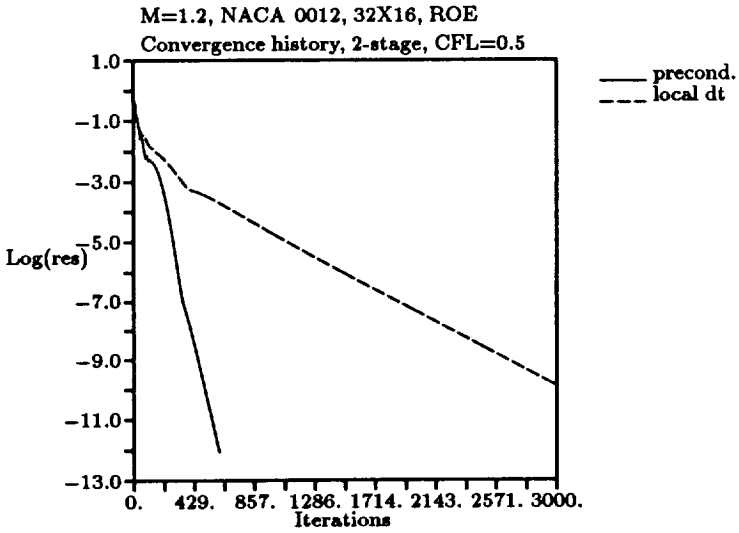

Figure 31: Residual-convergence histories for the computation of the solution of Figure 30 and the corresponding solution without preconditioning.

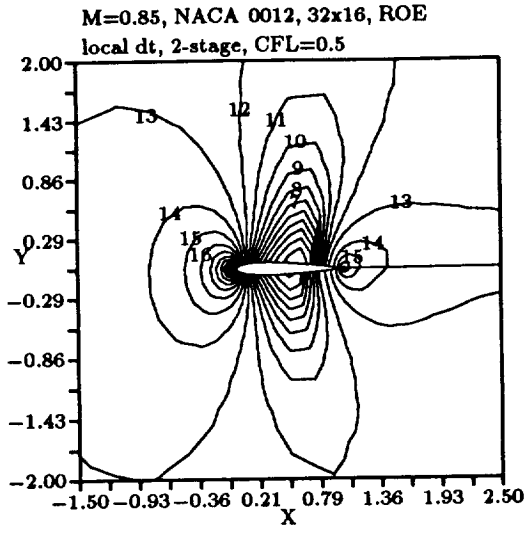

Figure 32: Steady solution of the Euler equations for flow over a NACA 0012 airfoil at $M_\infty = 0.85$, $\alpha = 1.0°$; shown are Mach-number contours. Local time-stepping was applied. Numerical flux function used: Roe's.

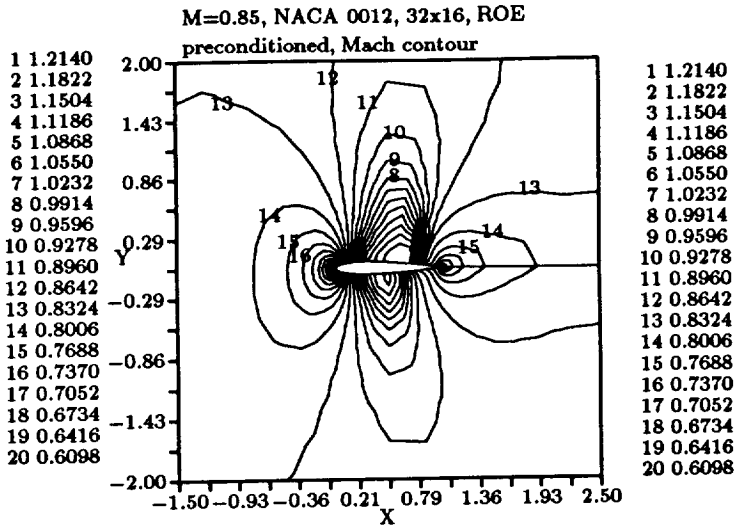

Figure 33: Steady solution of the Euler equations for flow over a NACA 0012 airfoil at $M_\infty = 0.85$, $\alpha = 1.0°$; shown are Mach-number contours. Matrix preconditioning was applied in combination with local time-stepping. Numerical flux function used: Roe's.

vergence rates after initial transients differ a factor 5.5.

For comparison the next pair of figures shows the steady solution obtained with Van Leer's flux-vector splitting (the regular and preconditioned schemes give identical results), and the two residual histories. The solution differs from the previous ones obtained with Roe's flux, illustrating the spread among first-order results on the present grid. The speed-up by preconditioning for the flux-split scheme is 5.0.

Figures 37 to 39 show solutions and residual histories for fully subsonic flow, $M_\infty = 0.5$, $\alpha = 0°$. At this Mach number the free-stream condition number reaches its minimum for subsonic flow, namely, 3; for lower Mach numbers the flow speed becomes the lowest characteristic speed, causing the condition number ($= 1 + 1/M$) to rise again. The condition number after preconditioning is 1.15, so a speed-up of a factor 2.6 is ex-

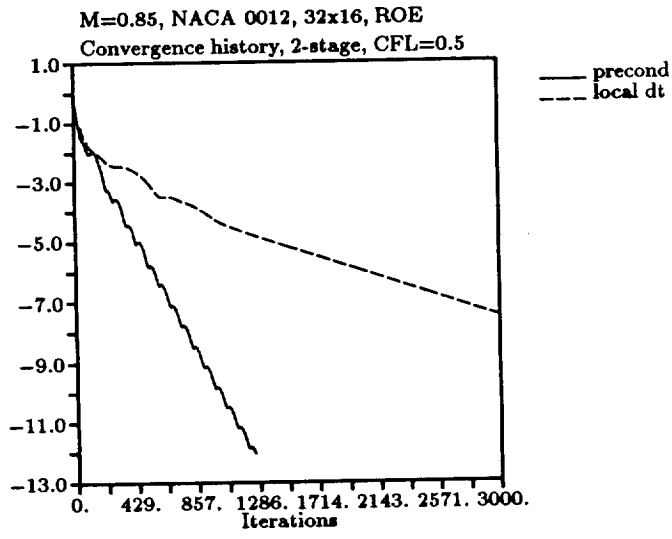

Figure 34: Residual-convergence histories for the computation of the solutions of Figures 32 and 33.

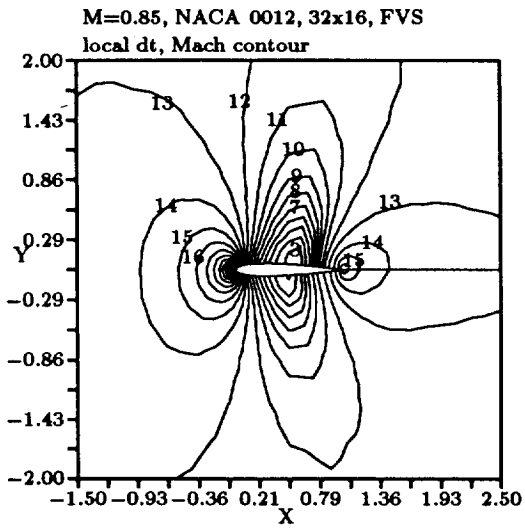

Figure 35: Steady solution of the Euler equations for flow over a NACA 0012 airfoil at $M_\infty = 0.85$, $\alpha = 1.0°$; shown are Mach-number contours. Numerical flux function used: Van Leer's. The regular and preconditioned schemes produce identical solutions.

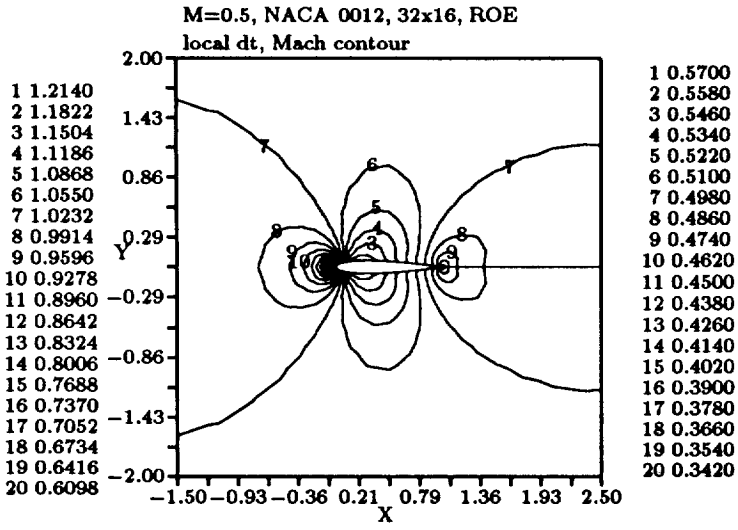

Figure 37: Steady solution of the Euler equations for flow over a NACA 0012 airfoil at $M_\infty = 0.5$, $\alpha = 0°$; shown are Mach-number contours. Local time-stepping was applied. Numerical flux function used: Roe's.

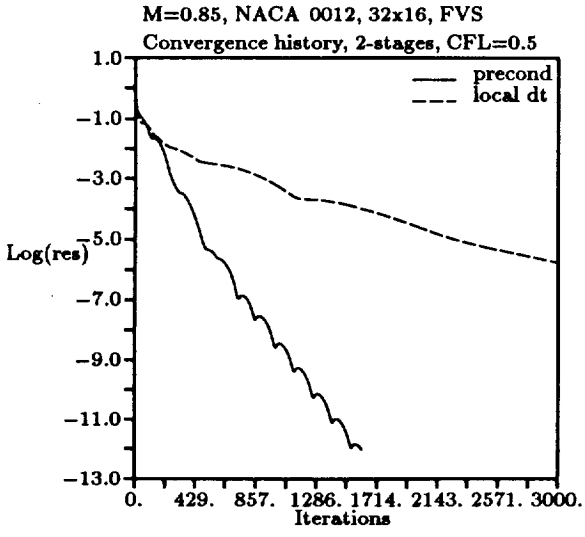

Figure 36: Residual-convergence histories for the computation of the solution of Figure 35 with the regular and preconditioned flux-vector split schemes.

pected. The actual speed-up in the later stages of convergence is 2.7; the closeness of agreement is probably accidental. The error on the airfoil surface for the preconditioned scheme has become quite prominent.

Figures 40 to 42, for $M_\infty = 0.1$, $\alpha = 0°$, demonstrate the ability of the preconditioning to remove the stiffness of the Euler equations in the limit of incompressible flow. Preconditioning reduces the condition number by a factor 11; the convergence histories indicate a factor 8.0 speed-up. The error at the surface in the solution by the preconditioned scheme is not worse than for $M_\infty = 0.5$, but the accuracy of the regular solution is now starting to degrade.

Finally, Figure 43 shows the two convergence histories for the case $M_\infty = 0.01$, $\alpha = 0°$. The kinetic energy of this flow is so small in comparison to its internal energy, that round-off errors in the computation of pressure from total energy are significantly raising

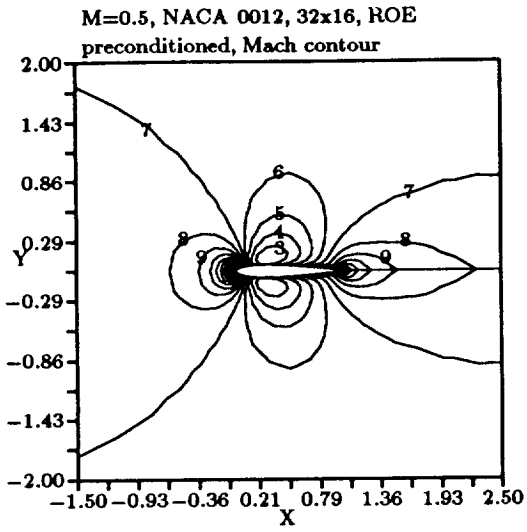

Figure 38: Steady solution of the Euler equations for flow over a NACA 0012 airfoil at $M_\infty = 0.5$, $\alpha = 0°$; shown are Mach-number contours. Matrix preconditioning was applied in combination with local time-stepping. Numerical flux function used: Roe's.

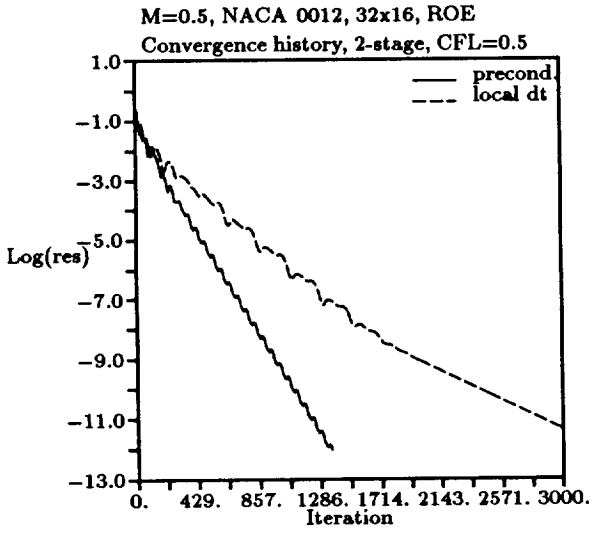

Figure 39: Residual-convergence histories for the computation of the solutions of Figures 37 and 38.

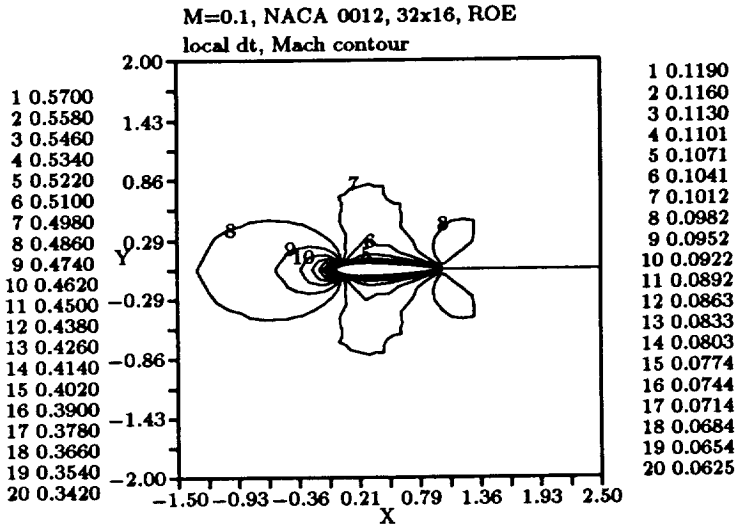

Figure 40: Steady solution of the Euler equations for flow over a NACA 0012 airfoil at $M_\infty = 0.1$, $\alpha = 0°$; shown are Mach-number contours. Local time-stepping was applied. Numerical flux function used: Roe's.

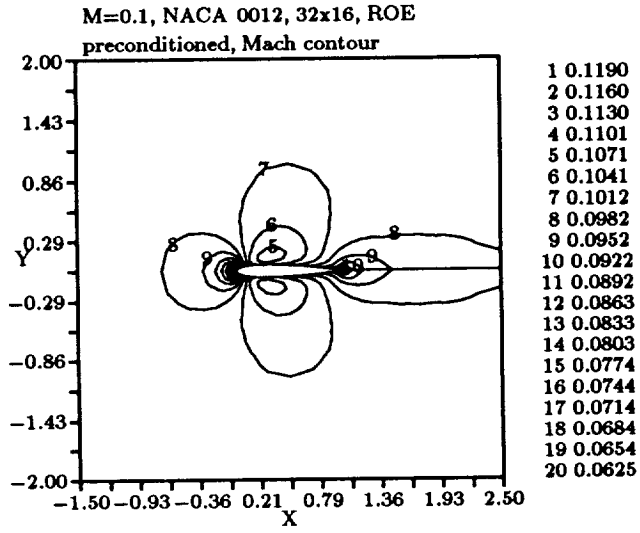

Figure 41: Steady solution of the Euler equations for flow over a NACA 0012 airfoil at $M_\infty = 0.1$, $\alpha = 0°$; shown are Mach-number contours. Matrix preconditioning was applied in combination with local time-stepping. Numerical flux function used: Roe's.

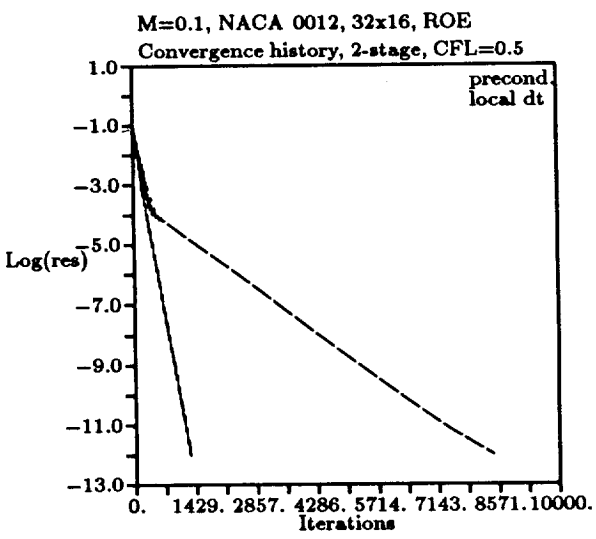

Figure 42: Residual-convergence histories for the computation of the solutions of Figures 40 and 41.

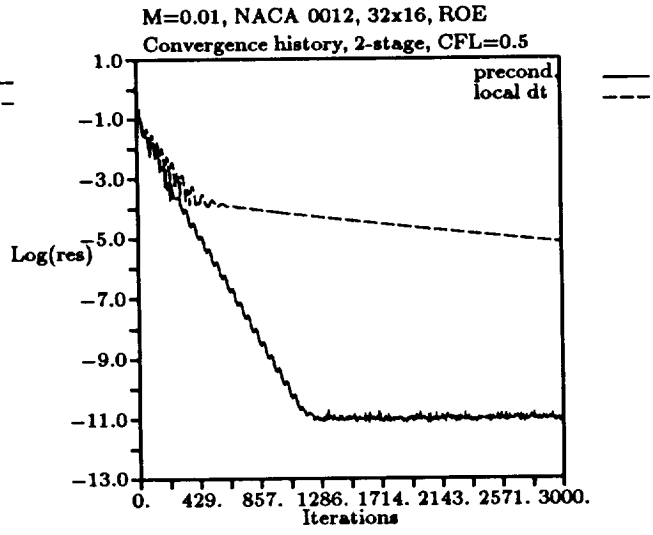

Figure 43: Residual-convergence histories for the computation of the steady flow about a NACA 0012 airfoil at $M_\infty = 0.01, \alpha = 0°$, without and with matrix preconditioning. Numerical flux function used: Roe's.

the value of "machine-zero." The preconditioned scheme produces a solution hardly different from the one for $M_\infty = 0.1$ (Figure 41), and achieves convergence in the same number of iterations; convergence without preconditioning is even slower than before. We did not pursue the regular solution until convergence; the non-converged solution is far-off. The theoretical speed-up by preconditioning, a factor 101, is not realized, because of the limiting of the time-step explained in Section 3.3.

The last examples are not intended for advocating the use of discretizations of the full compressible Euler equations for low-speed irrotational flows. The entropy and vorticity disturbances, convected so swiftly owing to the preconditioning, need not be there in the first place. Still, it is remarkable that an explicit scheme can produce steady solutions of the Euler equations on a given grid in a limited time for the entire range of flow speeds.

4 Three-dimensional preconditioning

When stepping up from two to three dimensions, some further deterioration of the condition number has to be accepted. The reason is that in three dimensions a new kind of shear wave is possible, namely, one that rotates the flow velocity; this wave mode can not be separated from the acoustic waves when manipulating the Euler equations. In consequence, when the acoustic waves are slowed down by a factor τ in the supersonic case, the 3-D shear wave is slowed down too. The condition number therefore deteriorates to $1/\sqrt{1-M^{-2}}$ for $M \downarrow 1$.

The preconditioning matrix for the 3-D Euler equations in a streamline-aligned coordinate system is similar to its two-dimensional

version in Equation (14):

$$\mathbf{P}_{3D} = \begin{pmatrix} \frac{\tau}{\beta^2}M^2 & -\frac{\tau}{\beta^2}M & 0 & 0 & 0 \\ -\frac{\tau}{\beta^2}M & \frac{\tau}{\beta^2}+1 & 0 & 0 & 0 \\ 0 & 0 & \tau & 0 & 0 \\ 0 & 0 & 0 & \tau & 0 \\ 0 & 0 & 0 & 0 & 1 \end{pmatrix}. \quad (22)$$

5 One-dimensional preconditioning revisited

It has been observed, in Section 2.2, that streamwise preconditioning for two-dimensional subsonic flow is not done with an generalization of the matrix used for one-dimensional flow. Inversely, though, the matrix $\mathbf{P}_{2D}$, can be reduced to a perfectly valid one-dimensional preconditioner, by taking $\tau = 1$ and removing its third row and column. Further analysis of symmetric matrices with the same sparsity brings to light that there exists a one-parameter family of one-dimensional preconditioning matrices, all capable of equalizing the characteristic speeds. Only one of these commutes with $\mathbf{A}$, and therefore preserves the eigenvector decomposition of the residual and the functional form of the characteristic variables; this is the common choice $|\mathbf{A}|^{-1}$ discussed in Section 2.1. The other prominent member of the family is the matrix derived from $\mathbf{P}_{2D}$; its special feature is that it minimizes the first diagonal element. This is essential for achieving optimal preconditioning for almost incompressible flow in two and three dimensions.

6 Conclusions and future developments

In the previous sections a local preconditioning matrix for the multi-dimensional Euler equations has been derived that reduces the spread of the characteristic speeds from a factor $(M+1)/\min(M, |M-1|)$ to a factor $1/\sqrt{1-\min(M^2, M^{-2})}$, where M is the Mach number. It has been shown that the latter value is the lowest attainable. Numerical experiments with this preconditioning, applied an explicit upwind discretization of the two-dimensional Euler equations, show that it significantly increases the rate of convergence to a steady solution, as predicted theoretically.

For a detailed account of the derivation, properties, and application of the preconditioning matrix the reader is referred to the second author's Ph.D. thesis [10].

At present the performance of the 2-D preconditioning matrix presented above is being tested in a variety of single-grid and multigrid Euler calculations, of first- and second-order accuracy. The emphasis is on two problems: removing the singularities of the preconditioning at $M = 1$ and $M = 0$ without losing robustness, and modifying numerical flux functions, if needed, for use with preconditioning. These are no trivial matters and may still require a considerable research effort.

The combination with multi-grid relaxation is particularly attractive, as the preconditioning can help to build marching schemes with better smoothing properties. Smoothing properties of Euler schemes have traditionally been analyzed on the basis of a scalar convection equation (see [11, 12, 13]) and are known to depend strongly on the Courant number employed. The effect of the preconditioning matrix on an Euler scheme is to equalize the Courant numbers associated with the different waves, so that optimal smoothing can be achieved simultaneously for all underlying characteristic convection schemes. Figures 44 and 45, taken from Van Leer et al. [14], show how the "Fourier footprint" of the two-dimensional first-order upwind-differencing operator clears up after preconditioning. The latter figure also con-

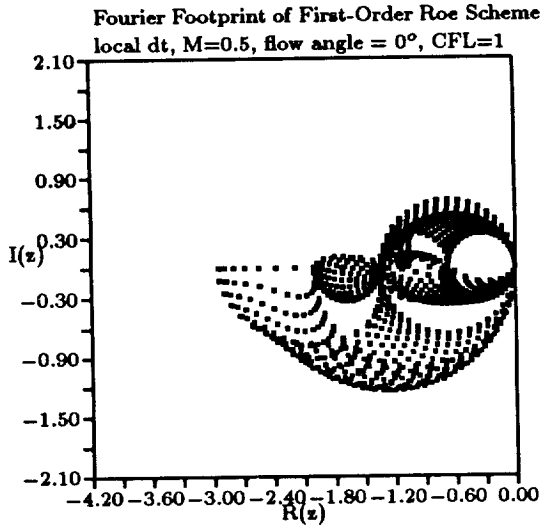

Figure 44: Fourier footprint (symbols) of the first-order upwind approximation of the spatial Euler operator, for $M = 0.5$, and flow speed aligned with the grid. The time-step chosen corresponds to a Courant-number value of 1.

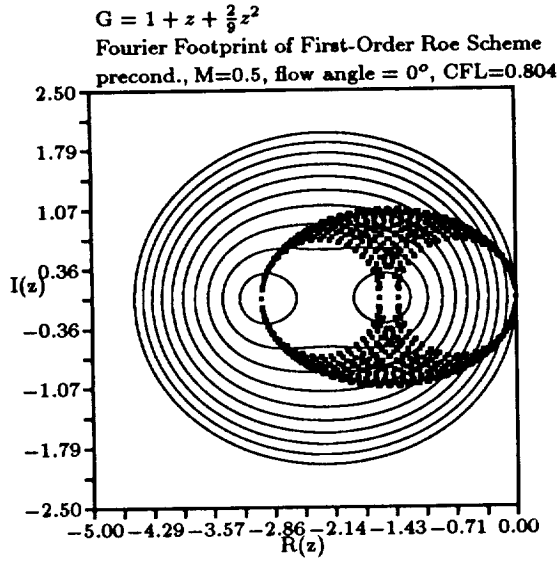

Figure 45: Fourier footprint (symbols) of the preconditioned first-order upwind approximation of the spatial Euler operator, for $M = 0.5$, and flow speed aligned with the grid. Also shown are level lines, up to the level 1, of the modulus of the polynomial $1 + z + \frac{2}{9}z^2$, associated with a particular two-stage time-marching scheme (see text). The zeros of the polynomial are placed in regions of the footprint where the high-high and high-low frequency combinations are concentrated. This coincidence requires the use of a special value of the time-step, corresponding to a Courant number of 0.804.

tains level lines, up to the level 1, of the modulus of the polynomial $1 + z + \frac{2}{9}z^2$, which is the amplification factor of the two-stage time-marching method

$$\tilde{\mathbf{U}} = \mathbf{U}^n + \frac{2}{9}\Delta t \mathbf{Res}(\mathbf{U}^n), \quad (23)$$

$$\mathbf{U}^{n+1} = \mathbf{U}^n + \Delta t \mathbf{Res}(\tilde{\mathbf{U}}). \quad (24)$$

Owing to the proper placement of the zeros of the amplification factor in the complex plane, and the proper choice of the time-step, strong high-frequency damping results when combining this marching method with the upwind residual.

It is expected that other iterative methods such as implicit marching methods, conjugate-gradient methods, and various vector-sequence convergence acceleration methods [15] will benefit from the clustering of eigenvalues accomplished by local preconditioning.

Another benefit expected of local preconditioning is that it will simplify convergence-accelerating boundary procedures such as developed by Karni [16] for the far field, and Roe and Mazaheri [17] for a solid wall. This simplification again is due to the circumstance that all error components travel at the same speed.

Presently under study is the inclusion of the cell aspect-ratio in the preconditioning matrix, in particular, in the value of τ. For stretched grids it is logical to equalize *cell crossing-times* rather than *wave speeds*; this can be accomplished by putting information about local cell geometry and flow angle into an extended definition of τ.

Inclusion of the cell aspect-ratio paves the way for local preconditioning of the Navier-Stokes equations. The interaction of the Euler preconditioning matrix with the terms representing physical dissipation so far has only been studied in one dimension (see Section 2.2).

Future directions of research may include the development and numerical testing of an optimal local preconditioning for other hyperbolic systems of equations, such as the lowest-order shallow-water equations and the equations of ideal magneto-hydrodynamics. While the former extension is trivial, the latter is complicated by the existence of an additional communication speed, the Alfvén speed, in the plasma.

It thus appears that the new analytic preconditioning has many potential uses in the development of Euler and Navier-Stokes algorithms. The present paper only marks its entrance into CFD.

Acknowledgements

The research reported here was supported in three different ways:

1. by NASA Langley Research Center under Grant NAG-1-869, monitored by Dr. James Thomas;
2. by NASA Langley Research Center through funding of the first author while in residence at ICASE during the summers of 1989 and 1990;
3. by NASA Lewis Research Center through funding of the first author while in residence at ICOMP during the summers of 1989 and 1990.

References

[1] B. van Leer, W. T. Lee, and K. G. Powell, "Sonic-point capturing," in *AIAA 9th Computational Fluid Dynamics Conference*, 1989.

[2] P. L. Roe, "Characteristic-based schemes for the Euler equations," *Annual Review of Fluid Mechanics*, vol. 18, pp. 337–365, 1986.

[3] B. van Leer, J. L. Thomas, P. L. Roe, and R. W. Newsome, "A comparison of numerical flux formulas for the Euler and Navier-Stokes equations," in *AIAA 8th Computational Fluid Dynamics Conference*, 1987.

[4] W. Coirier and B. van Leer, "Numerical flux functions for the Euler and Navier-stokes equations ii. progress in flux-vector splitting," in *AIAA 10th Computational Fluid Dynamics Conference*, 1991.

[5] E. Turkel, "Acceleration to a steady state for the Euler equations." ICASE Report 84-32, 1984.

[6] E. Turkel, "Preconditioned methods for solving the incompressible and low speed compressible equations." ICASE Report 86-14, 1986.

[7] B. van Leer, "Flux-vector splitting for the Eulerequations," *Lecture Notes in Physics*, vol. 170, 1982.

[8] A. Jameson, W. Schmidt, and E. Turkel, "Numerical solutions of the Euler equations by a finite-volume method using Runge-Kutta time-stepping schemes," AIAA Paper 81-1259, 1981.

[9] AGARD Subcommittee C, "Test cases for inviscid flow field methods." AGARD Advisory Report 211, 1986.

[10] W.-T. Lee, *Local Preconditioning of the Euler Equations.* PhD thesis, University of Michigan, 1991.

[11] A. Jameson, "Numerical solution of the Euler equations for compressible inviscid fluids," in *Numerical Methods for the Euler Equations of Fluid Dynamics* (F. Angrand, A. Dervieux, J. A. Désidéri, and R. Glowinski, eds.), SIAM, 1985.

[12] B. van Leer, C. H. Tai, and K. G. Powell, "Design of optimally-smoothing multi-stage schemes for the Euler equations," in *AIAA 9th Computational Fluid Dynamics Conference*, 1989.

[13] C.-H. Tai, *Acceleration Techniques for Explicit Euler Codes.* PhD thesis, University of Michigan, 1990.

[14] B. van Leer, W. T. Lee, P. L. Roe, C.-H. Tai, and K. G. Powell, "Design of optimally smoothing multi-stage schemes for the Euler equations," in *Fifth Copper Mountain Conference om Multigrid Methods*, 1991.

[15] D. A. Smith, W. F. Ford, and A. Sidi, "Extrapolation methods for vector sequences," *SIAM Review*, vol. 29, 1987.

[16] S. Karni, "Accelerated convergence to steady states by gradual far-field damping," in *AIAA 10th Computational Fluid Dynamics Conference*, 1991.

[17] K. Mazaheri and P. L. Roe, "New light on numerical boundary conditions," in *AIAA 10th Computational Fluid Dynamics Conference*, 1991.